J Mol Model (2009) 15:1397–1405
DOI 10.1007/s00894-009-0505-2

ORIGINAL PAPER

Catalytic activities of dismution reactions of $Cu(bpy)Br_2$ compound and its derivatives as SOD mimics: A theoretical study

Qingxia Lu · Xichen Li · Yan Wang · Guangju Chen

Received: 2 February 2009 / Accepted: 14 March 2009 / Published online: 7 May 2009

Abstract The systematical investigations on the catalytic mechanisms of dismutation reactions for the superoxide dismutase (SOD) mimics of $Cu(bpy)Br_2$ and its derivatives $Cu(L^1)Br_2$ and $Cu(L^2)Br_2$ (bpy=2,2'- dipyridyl, L^1=5,5'- di [1- (triethylammonio)methyl]- 2,2'- dipyridyl cation and L^2=5,5'- di [1- (tributylammonio)methyl]- 2,2'- dipyridyl cation) have been carried out by the DFT/UB3LYP method. The catalytic reaction for each of these compounds is confirmed to be a redox cycle consisting of two half-reactions. In the first half-reaction, a proton is transferred from hydroperoxide neutral radical (·OOH) to one nitrogen atom of pyridinic ring with Cu(II) being reduced to Cu(I) in the meantime. In the second half-reaction, the proton is transferred back to another hydroperoxide radical (·OOH) to form hydrogen peroxide molecule, oxidizing Cu(I) back to its initial state. Our results show that the first half-reaction for all reactions is the rate-controlling step with the forward barrier values of 6.61, 4.84, 3.79 kcal·mol^{-1} for $Cu(bpy)Br_2$, $Cu(L^1)Br_2$, and $Cu(L^2)Br_2$, respectively. Consequently, the SOD-like activities of the three mimics are in the order of $Cu(bpy)Br_2$ < $Cu(L^1)Br_2$ < $Cu(L^2)Br_2$. The effect factors on the SOD-like activity for the studied compounds have also been discussed.

Keywords Dismutation mechanism · DFT/UB3LYP · SOD-like activity · Superoxide dismutase

Q. Lu · X. Li · Y. Wang (✉) · G. Chen (✉)
College of Chemistry, Beijing Normal University,
Beijing 100875, P. R. China
e-mail: wangy@bnu.edu.cn
e-mail: gjchen@bnu.edu.cn

Introduction

Superoxide dismutases (SODs), the ubiquitous metalloenzymes, can reduce oxidative stress in the intracellular environment through preventing oxidative damage of a highly toxic species of superoxide radical anion ($O^{\bullet-}_2$) [1]. They play a key role in combating a broad range of diseases, such as ischemic-reperfusion injury, inflammation, diabetes, neuronal degeneration, cancer, aging, AIDS, and familial amyotrophic lateral sclerosis (FALS) [2–6]. Three types of SODs have been classified by their cofactor metal ions so far, i.e., Cu- and Zn- dependent SODs (CuZnSODs) [7], Fe- or/and Mn-dependent SODs (Fe/MnSODs) [8], and Ni-dependent SODs (NiSODs) [9]. CuZnSODs are the most abundant in living nature [10–12]. The mechanism by which SODs catalyze the conversion of toxic $O^{\bullet-}_2$ radicals to dioxygen and hydrogen peroxide molecules is generally thought as follows:

$$2O_2^{\bullet-} + 2H^+ \xrightarrow{SOD} O_2 + H_2O_2$$

Valentine's group has contributed a lot of information in researching various kinds of SODs [13–17]. Pelmenschikov and Siegbahn etc. have also systematically investigated the catalyzing mechanisms of a series of natural SODs by theoretical calculations [7, 9]. The dismutation reaction mechanism of SOD complexes is generally accepted as a redox cycle with two half-reactions. In the first half-reaction, a SOD complex combines a hydroperoxyl radical (·OOH) around its copper center as a complex reactant, followed by the proton transfer process to form a dioxygen (O_2) molecule and a intermediate product with Cu(II) reduced to Cu(I). In the second half-reaction, the intermediate product binds another hydroperoxyl radical (·OOH) as a second complex

reactant, then the initial SOD complex is reproduced *via* an inverse proton transfer process, and H_2O_2 molecule is formed with Cu(I) oxidized back to Cu(II) at one time. Most studies have shown that the copper ion is the active-site center [13, 18], and positively-charged residues of amino acids (such as ammonium and guanidine groups) can markedly increase the reaction activity [19–21].

Although natural SODs have been accepted as the antioxidative therapeutic agents, there remain some major drawbacks, such as the large molecular weight, immunological problems and difficulties in traversing or penetrating membrane barriers to reach target sites. Therefore, many artificial SOD mimics, bearing not only similar SOD activities but also favorable structural and functional merits, have been extensively studied and synthesized as pharmaceutical candidates [22]. Interestingly, mononuclear Cu(II) complexes have attracted increasing attention to their small molecular weight and efficient activities as the SOD mimics. Moreover, they have been considered as potentially good and simple models for both simulating the superoxide dismutase activity and understanding the more complicated metalloproteins. For example, Mao'group has designed and synthesized some SOD-mimetic compounds with high SOD-like activity [23, 24]. Moreover, many charged copper(II) complexes with the ligands 5,5'- di[1- (triethylammonio)methyl]- 2,2'- dipyridyl and 5,5'- di[1- (tributylammonio)methyl]- 2,2'- dipyridyl have been synthesized so far [25–27]. Especially, bipyridine ligands and its derivatives may form 1:1 or 1:2 copper complexes. To the best of our knowledge, the catalytic reactions and properties of these complexes have not yet been systematically and theoretically investigated so far.

Considering the importance of understanding the effects of different ligands on SOD-like activities, it is necessary to study systematically a series of SOD mimics with main ligands and their derivatives at a molecular level. In this work, we employed DFT/UB3LYP method to study the catalytic mechanisms and activities of $Cu(bpy)Br_2$ (bpy=2,2'- dipyridyl) [28, 29] and their two derivatives $Cu(L^1)Br_2$ and $Cu(L^2)Br_2$ (L^1=5,5'- di[1- (triethylammonio) methyl]- 2,2'- dipyridyl), L^2=5,5'- di[1- (tributylammonio) methyl]- 2,2'- dipyridyl) complexes, as SOD mimics [25–27]. Our research goals are: 1) to reveal SOD-like activity of three SOD mimics theoretically and to compare with the experimental results; 2) to address possible factors to affect SOD-like activity of the compounds with different ligands. The investigated results of catalytic properties for these compounds will provide an insight into understanding potential SOD-like activities of other similar SOD mimics involving the redox dismutation reaction.

Computational details

The geometries of $Cu(bpy)Br_2$ complex and two of their derivatives, $Cu(L^1)Br_2$ and $Cu(L^2)Br_2$ complexes, were fully optimized at the DFT/UB3LYP level to determine all of the stable and saddle-point structures for the dismutation mechanisms [30–32]. The calculations were carried out with a mixed basis set: the LanL2DZ (double-ξ quality) with Los Alamos effective core potentials (ECPs) for copper atom [33–35] and 6-311G(d,p) basis set for the other atoms. Furthermore, the large basis set SDD with the Stuttgart-Dresden ECP has been employed for copper atom to optimize the geometries and to calculate further the energies for $Cu(bpy)Br_2$ complex. The improvement of the basis set has little influence on geometries and relative energies, i.e., the deviation of bond lengths and bond angles are less than 2%, and the deviation of reaction barriers are less than 5%. Taking an acceptable computational cost into account, the mix basis set of 6-311G(d,p)+LanL2DZ was used for further calculations. For the biradical systems, the unrestricted DFT/UB3LYP method was employed to calculate the electronic properties of the complexes with triplet and singlet spin states.

Frequency calculations for all stationary points were carried out at the optimized basis set level to obtain Gibbs free energies and to determine whether a given structure is a minimum or a transition state (TS). All initial SOD mimics, intermediates and final products have only real harmonic frequencies, and each transition state has only a single imaginary frequency which corresponds to the vibrational model of hydrogen proton transferring. To understand the properties of the complexes, the solvent (water) effect is considered as an important factor for reaction mechanism

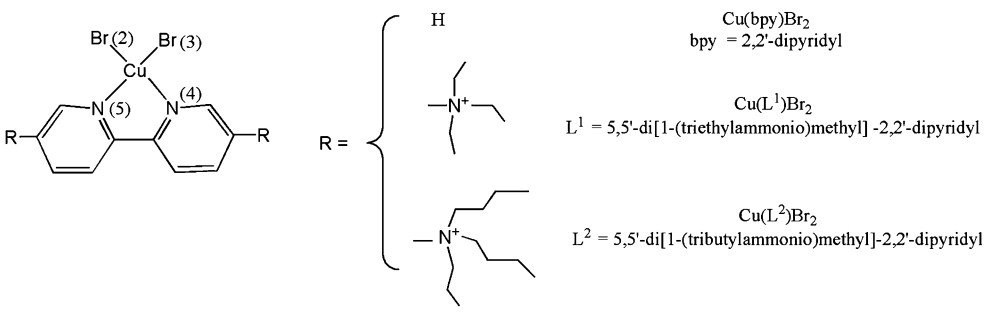

Fig. 1 Scheme of structures of $Cu(bpy)Br_2$, $Cu(L^1)Br_2$, $Cu(L^2)Br_2$ compounds

calculations. The solvation energy calculations for all reaction processes were performed with IEFPCM/UAKS model [36–40]. The electronic properties of the stationary points were also studied using the natural bond orbital (NBO) analysis [41–44]. To improve the energy properties, we employed a large mix basis set of LanL2DZ for copper atom and 6-311++G(2df,2pd) for other atoms to refine the reaction barriers. The results show that the refined forward barriers at the larger mix basis set level are lower by 5% than those at the optimized basis set level. Therefore, it is clear that the energies obtained at the original basis set level are reliable. All of our calculations were carried out by using Gaussian 03 program [40].

Results and discussion

Geometries of the SOD mimic complexes

The scheme of structures for the studied SOD mimic compounds is shown in Fig. 1 with the corresponding symbols and labels for the key atoms. The computed key bond lengths and angles for the optimized geometries of the studied complexes are shown in Table 1. The optimized structures of the complexes show that the Cu(II) ion in each complex is coordinated by two nitrogen atoms of a ligand and two bromine atoms with *cis*-planar characteristics (see Fig. 1 and Table 1). The structures of center area close to Cu atoms for all complexes are quite similar, except for two bipyridyl ligands of $Cu(L^1)Br_2$ or $Cu(L^2)Br_2$ complex linking to bulky quaternary ammonium groups. We can see from Table 1 that the Cu – N or Cu – Br distances in each complex are almost equivalent due to their ligands with C_2 axis symmetry. Namely, the average Cu-N and Cu-Br bonds for $Cu(bpy)Br_2$, $Cu(L^1)Br_2$ and $Cu(L^2)Br_2$ complexes are the values of 2.134, 2.142, 2.155 Å and 2.401, 2.387, 2.393 Å, respectively. The calculated Cu-Br distances are consistent with the normal Cu-halogeno atom distances reported by the experiments. Interestingly, the increase of substitute chain lengths induces the increase of Cu-N distances in these complexes, which may facilitate the center Cu atom combining a substrate presented in the dismutation reaction.

Dismutation mechanisms of the SOD mimics

Based on the previous mechanism discussion [7, 9], we have investigated the dismutation reaction pathways and activities of three SOD-mimic compounds. Considering the fact that both two nitrogen atoms and two bromine atoms may function as the acceptors of the transferred proton, we have successfully found the most practicable pathway of catalytic reaction theoretically. Namely, the pathway of a proton transferring to a bromine atom is invalidate due to causing the releasing of a hydrogen bromide (HBr) molecule, then preventing the proceeding of second half reaction. Therefore, only energetically favorable dismuta-

Table 1 Selected optimized parameters (distances: Å; angles: degree) of all stable complexes (only triplet states for the first half-reactions)

		$Cu(bpy)Br_2$	$Cu(L^1)Br_2$	$Cu(L^2)Br_2$
SODM	Cu-Br(2)	2.401	2.387	2.392
	Cu-Br(3)	2.400	2.387	2.393
	Cu-N(4)	2.134	2.142	2.154
	Cu-N(5)	2.133	2.141	2.156
R1	Cu-O(6)	2.226	2.231	2.225
	O(6)-O(7)	1.320	1.320	1.320
	O(7)-H(8)	1.023	1.013	1.019
	N(4)—H(8)	1.654	1.709	1.677
	N(4)——O(7)	2.673	2.715	2.689
	N(4)-H(8)-O(7)	174.4	171.4	171.4
TS1	Cu-O(6)	2.057	2.037	2.044
	O(6)-O(7)	1.302	1.299	1.301
	O(7)——H(8)	1.279	1.145	1.141
	N(4)—H(8)	1.215	1.370	1.375
	N(4)——O(7)	2.493	2.500	2.501
	N(4)-H(8)-O(7)	176.1	167.3	167.2
P1	Cu-O(6)	3.258	3.361	3.455
	O(6)-O(7)	1.207	1.206	1.206
	O(7)——H(8)	3.197	2.285	2.305
	N(4)-H(8)	1.045	1.030	1.030
	N(4)——O(7)	3.373	3.116	3.122
	N(4)-H(8)-O(7)	90.6	136.8	135.3
R2	Cu-O(9)	1.977	1.973	1.964
	O(9)-O(10)	1.418	1.419	1.426
	O(9)—H(8)	1.524	1.391	1.443
	N(4)-H(8)	1.090	1.140	1.121
	N(4)——O(7)	2.593	2.516	2.530
	N(4)-H(8)-O(7)	165.1	167.4	161.1
TS2	Cu-O(9)	1.954	1.975	1.961
	O(9)-O(10)	1.449	1.429	1.430
	O(9)—H(8)	1.347	1.319	1.408
	N(4)—H(8)	1.163	1.181	1.144
	N(4)——O(7)	2.498	2.487	2.519
	N(4)-H(8)-O(7)	168.7	168.4	161.6
P2	Cu-O(9)	3.252	2.130	2.215
	O(9)-O(10)	1.449	1.451	1.455
	O(9)-H(8)	0.982	1.003	0.986
	N(4)—H(8)	3.490	1.711	1.851
	N(4)——O(7)	3.696	2.673	2.720
	N(4)-H(8)-O(7)	94.3	159.5	145.2

Note: **SODM** means the initial superoxide dismutase mimic; **R1**, **TS1**, **P1** and **R2**, **TS2**, **P2** stand for reactants, transition states and products in the first-half reaction and second-half reaction, respectively

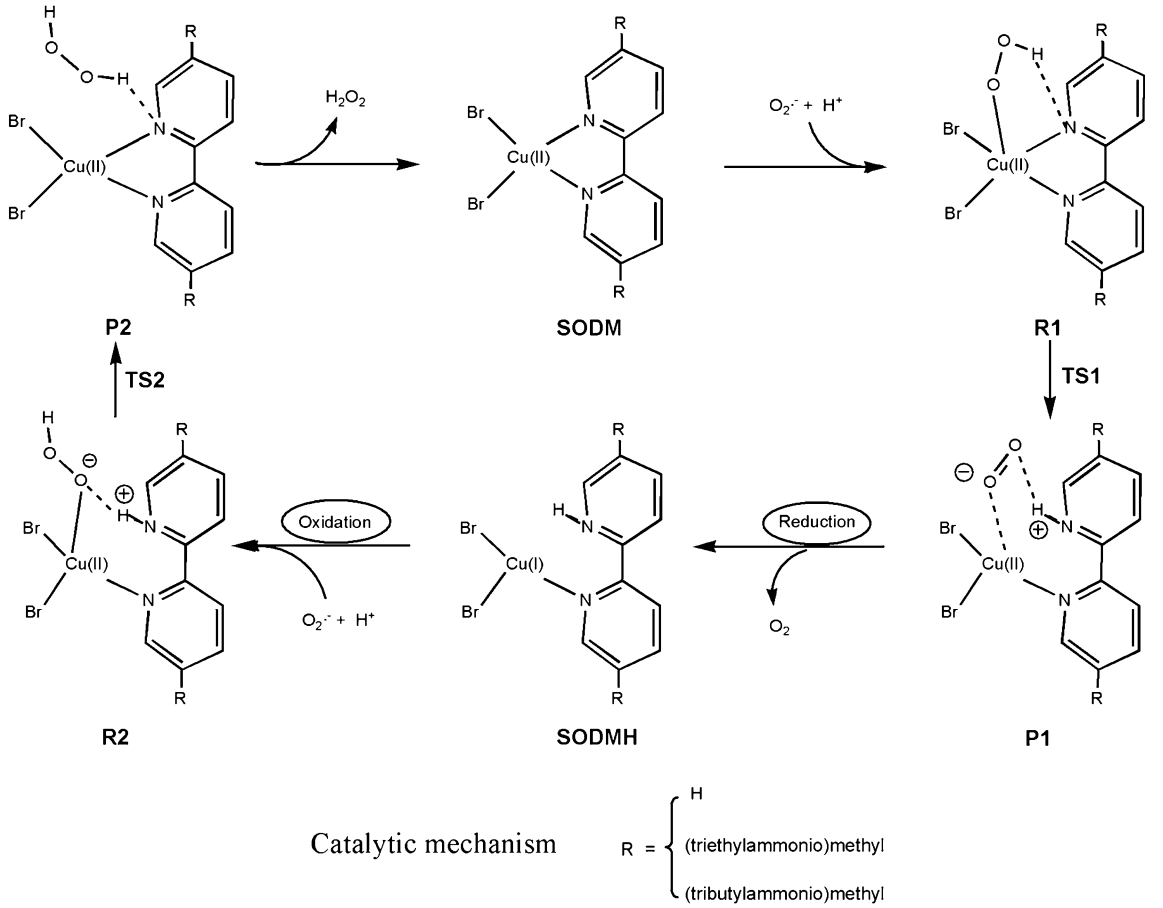

Fig. 2 Scheme of dismutation catalytic mechanism

tion pathways involving a proton transferring to a nitrogen atom for these SOD mimic compounds have been presented in this paper. In addition, in consideration of the biradical characteristics for some stationary points in the first half-reaction, the triplet and singlet state calculations of these studied SOD mimics for the investigated mechanisms were also carried out at the open-shell DFT/UB3LYP level. The results indicate that the reaction mechanisms with the triplet states are energetically favorable. The calculated data, therefore, only with the triplet states for the first half-reactions have been shown in this paper.

The scheme of catalytic reaction mechanisms and all calculated TS structures are shown in Figs. 2 and 3, respectively. The computed critical bond lengths and angles for the optimized geometries of all stationary points are given in Table 1. The forward barriers (the difference of Gibbs free energies between a reactant and a transition state) of two half-reactions for all studied compounds are shown in Table 2. In the first half-reaction of $Cu(bpy)Br_2$ compound, the **SODM** compound combines a hydroperoxyl neutral radical (·OOH) at the axial direction of Cu-ligand plane to form a complex reactant (**R1**) (see Fig. 2). Then, the H(8) atom of ·OOH in **R1** is transferred to N(4) atom of pyridinic ring to form the product (**P1**) *via* the transition state of H-transformation (**TS1**) (see Fig. 3). Namely, the O(6) of ·OOH in the **R1** complex coordinates to Cu atom with Cu-O(6) distance of 2.226 Å, and the H(8) atom binding to O(7) atom points to N(4) atom of pyridinic ring with N(4)-H(8) distance of 1.654 Å (see Table 1). At the **TS1** complex, H(8) is localized between N(4) and O(7) atoms with the N(4)-H(8) distance of 1.215 Å and the O(7)-H(8) distance of 1.279 Å (see Fig. 3 and Table 1). The imaginary vibrational frequency mode confirms that **TS1** is the correct transition state corresponding to the H(8) transferring from the hydroperoxyl neutral radical to the N (4) atom. The corresponding NBO orbitals relative to the interactions are shown in Fig. 4. For the **P1** complex, H(8) atom binds to N(4) atom with the N(4)-H(8) distance of 1.045 Å and the O(7)-H(8) distance of 3.197 Å (see Table 1). Interestingly, the O(6)-O(7) distance of 1.207 Å is similar to that of normal oxygen molecule (O_2), which is favorable for the release of O_2 molecule from **P1**, and consequently for forming another intermediate compound, **SODMH**. The calculated forward Gibbs barrier for the first half-reaction is 6.61 kcal·mol^{-1}. In the second half-reaction, the **SODMH** produced from the **P1** complex in the first

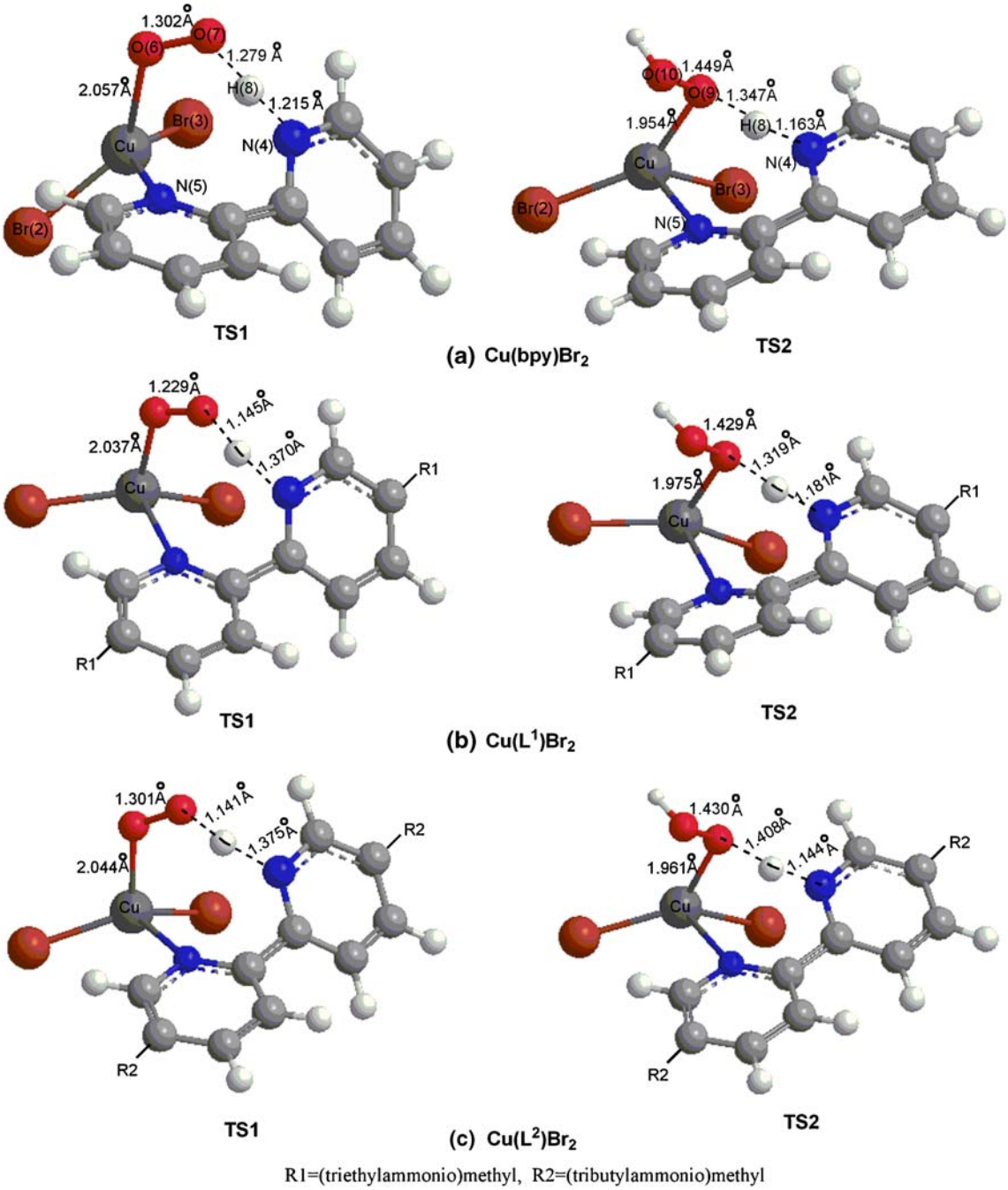

Fig. 3 Optimized **TS1** and **TS2** structures for three studied compounds

half-reaction combines another ·OOH radical at the same direction as in the first half-reaction to form a complex reactant (**R2**) (see Fig. 2). The positive charges on the Cu ion can be considered as a drive force for the combination of ·OOH radical for **SODM** (**R1**) and **SODMH** (**R2**) reactants. Then, H(8) atom bound to N(4) atom in the **R2** complex is transferred inversely to O(9) atom of ·OOH to form the product (**P2**) *via* a transition state of H-transformation (**TS2**). In detail, the O(9) atom of **R2** complex coordinates to Cu cation with Cu-O(9) distance of 1.977 Å, and the H(8) atom points to O(9) atom with O(9)-H(8) distance of 1.524 Å (see Fig. 3 and Table 1). At **TS2**, H(8) atom is localized between N(4) and O(9) atoms with the N(4)-H(8) distance of 1.163 Å and the O(9)-H(8) distance of 1.347 Å. The imaginary vibrational frequency mode also confirms that **TS2** is the correct transition state corresponding to the H(8) transferring reversely to the O(9) atom. The corresponding NBO orbitals relative to the interactions are shown in Fig. 4. For the **P2** complex, H(8) atom bonds to O(9) atom with the O(9)-H(8) distance of

Table 2 Relative Gibbs free energies (kcal·mol^{-1})

	$Cu(bpy)Br_2$	$Cu(L^1)Br_2$	$Cu(L^2)Br_2$
R1	0.0	0.0	0.0
TS1	6.61	4.84	3.79
P1	−12.76	−6.26	−6.98
R2	0.0	0.0	0.0
TS2	4.24	2.00	0.85
P2	−18.10	−10.27	−5.13

0.982 Å and the N(4)-H(8) distance of 3.490 Å, which presents the configuration of HOOH molecule binding to the Cu cation of $Cu(bpy)Br_2$ compound. In particular, the O(9)-O(10) distance in the **P2** complex is similar to the normal O-O single bond in a hydrogen peroxide molecule (H_2O_2) molecule, which is favorable for the release of a H_2O_2 molecule from the **P2** complex. The calculated forward Gibbs barrier for the second half-reaction is about 4.24 kcal·mol^{-1}. In the following step, a H_2O_2 molecule releases from **P2** to form the initial structure of $Cu(bpy)Br_2$ compound and an isolated H_2O_2 molecule. The calculated forward Gibbs barrier for the H_2O_2 releasing from this step is 2.79 kcal·mol^{-1}, which is lower than the first step barrier. In summary, two studied half-reactions achieve a full redox cycle of dismutation mechanism for $Cu(bpy)Br_2$ compound, and the first half-reaction is the rate-controlling step.

The dismutation mechanisms for $Cu(L^1)Br_2$ and $Cu(L^2)Br_2$ compounds have also been studied in the present work. The dismutation mechanisms are similar to that of $Cu(bpy)Br_2$ compound. Similar central structures of **R1**, **TS1**, **P1**, **R2**, **TS2** and **P2** have been confirmed in these reaction processes. The rate-controlling step for each of these compounds is also the first half-reaction with the forward barrier values of 4.84 and 3.79 kcal·mol^{-1} for $Cu(L^1)Br_2$ and $Cu(L^2)Br_2$ compound, respectively (see Table 2). With regards to the calculations of the triplet and singlet states for these complexes involved in the first half-reaction pathways, the calculated forward barriers of the singlet states for these complexes are higher than those of the triplet states. So the stable triplet states of these stationary points during the first half-reaction pathways represent significantly the biradical characteristics of the dismutation mechanisms. In addition, the present studies predict the barriers of just 3~7 kcal mol^{-1} for the $Cu(bipy)Br_2$ derivatives are much smaller than those of the previous studies of $Cu(Im)_4$ core complex with the barriers on the order of 13-18 kcal mol^{-1} reported by Siegbahn et al. [7]. This can be explained by the fact that the steric hindrance is much smaller for $Cu(bipy)Br_2$ and its derivatives, and the dimensional bulk of four-Im-ring ligands surrounding copper ion for $Cu(Im)_4$ core complex is larger, although the active-site model with its $Cu(Im)_4$ core is simplified. Furthermore, the configuration flexibility of the present $Cu(bipy)Br_2$ and its derivatives can facilitate the catalytic reactivity; whereas the three-Im-ring ligands of four Im rings in $Cu(Im)_4$ core complex are linked by some hydrogen bonds in active-site model, which prevents from its flexible ability.

Reactive activities of the SOD mimics

The relative Gibbs energies with respect to the corresponding reactants are shown in Table 2. It can been seen from Table 2 that the forward barriers in the rate-limiting steps for $Cu(bpy)Br_2$, $Cu(L^1)Br_2$ and $Cu(L^2)Br_2$ compounds are in the order of $Cu(bpy)Br_2$>$Cu(L^1)Br_2$>$Cu(L^2)Br_2$, which induces the SOD-like activity order of $Cu(bpy)Br_2$<$Cu(L^1)Br_2$<$Cu(L^2)Br_2$. Such trend is consistent with the experimental results indicated by the IC_{50} values and the second-order rate constants in the experiment [27]. Interestingly, the reaction forward barriers of the derivatives $Cu(L^1)Br_2$ and $Cu(L^2)Br_2$ compounds are much lower by 27% and 43% than that of $Cu(bpy)Br_2$ compound,

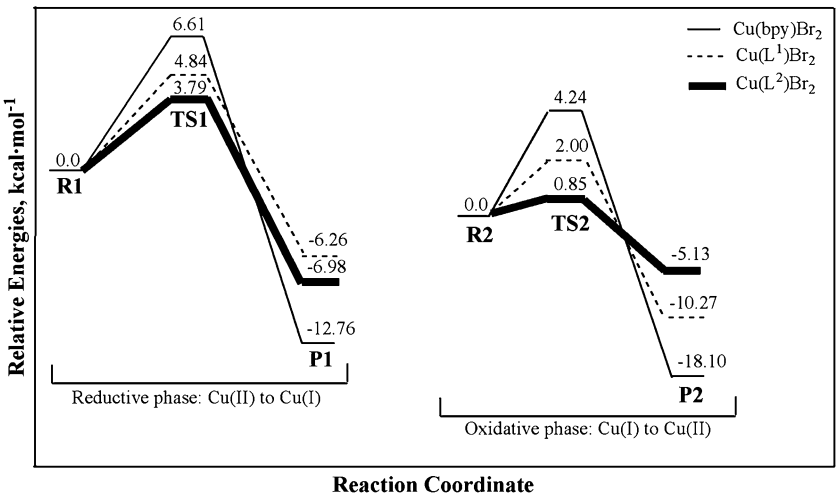

Fig. 4 Profile of relative Gibbs free energies for three reactions

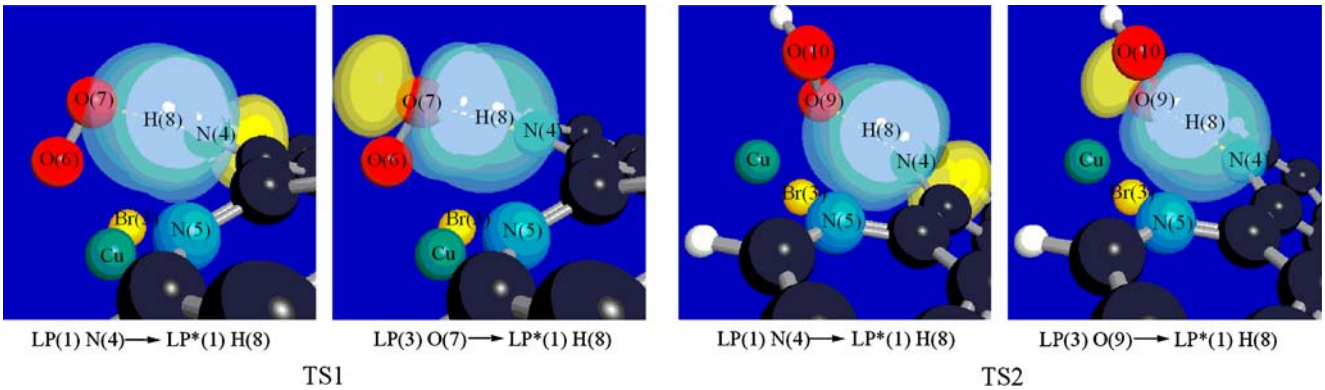

Fig. 5 Some NBO orbitals of **TS1** and **TS2** for Cu(bpy)Br_2 compound

respectively. Their energy profile is shown in Fig. 5. Consequently, their SOD-like activities are much higher than Cu(bpy)Br_2 compound. According to the natural orbital population analysis (NPA) in the present work, the reason can be explained by the fact that the highly positive charges located at the ligands L^1 and L^2 facilitate the hydrogen transfer. In addition, the substitute groups (triethylammonio and tributylammonio) in the ligands L^1 and L^2 with the positive charges, which is similar to the Arg141 aminophenol residue of the nature CuZnSOD molecule with the positive charge, present reasonably high SOD-like activities as SOD mimics [27]. Moreover, the solvent effect is also an important factor for the reaction activities of the compounds. The differences of calculated solvent polarization energies between the reactants and transition states ($\Delta E_{solv} = E_{solv(\mathbf{TS})} - E_{solv(\mathbf{R})}$) have been shown in Table 3. The $\Delta E_{solv1\ [Cu(L1)Br2]}$ is larger than $\Delta E_{solv1\ [Cu(L2)Br2]}$ in the first-half reactions, which can explain that the SOD-like activity of Cu(L^2)Br_2 compound is higher than Cu(L^1)Br_2 compound because the smaller the ΔE_{solv} is, the lower the forward barrier is. Similarly, the $\Delta E_{solv2\ [Cu(L1)Br2]}$ is still larger than $\Delta E_{solv2\ [Cu(L2)Br2]}$ in the second-half reactions (see Table 3 and Fig. 5). For the structural changes during the reaction processes, the O(7)-H(8) distances with the hydrogen transferring from **R1** to **TS1** elongate 0.256 Å, 0.132 Å and 0.122 Å for Cu(bpy)Br_2, Cu(L^1)Br_2 and Cu(L^2)Br_2 compounds, respectively. Synchronously, the separated angles of two pyridine ring planes from **R1** to **TS1** enlarge 4.8, 6.5 and 10.8 degrees for Cu(bpy)Br_2, Cu(L^1)Br_2 and Cu(L^2)Br_2 compounds, respectively. The change characteristics of these structural parameters from **R1** to **TS1** predict that the SOD-like active trend of the compounds, Cu(bpy)Br_2<Cu(L^1)Br_2<Cu(L^2)Br_2. On the other hand, the configuration flexibility of complexes can still affect SOD-like activity due to the conformation change of SOD mimics facilitating to receive a transferred hydrogen atom in a dismutation reaction process. Consequently, the substitute group of tributylammonio in L^2 group is longer than triethylammonio in L^1 group, which causes the great configuration flexibility of Cu(L^2)Br_2 compound during the reaction process, and ultimately, the higher SOD-like activity.

In addition, according to the natural orbital population analysis (NPA), the net charge populations on the central Cu cations of all studied complexes are shown in Table 4. It can been seen from Table 4 that the positive charges on Cu cations of the stationary points decrease gradually during each first-half reaction process and increase gradually in the second-half reaction. So Cu cation is reduced in the first half-reaction, and is oxidized back to its initial state in the second half-reaction, which indicates furthermore that the catalytic mechanism studied in the present work is reasonable for a redox cycle of dismutation reactions.

Table 3 The solvent energies (kcal·mol^{-1})

	$E_{solv(\mathbf{R1})}$	$E_{solv(\mathbf{TS1})}$	ΔE_{solv1}	$E_{solv(\mathbf{R2})}$	$E_{solv(\mathbf{TS2})}$	ΔE_{solv2}
Cu(L^1)Br_2	−130.56	−124.53	6.03	−127.88	−126.14	1.74
Cu(L^2)Br_2	−111	−106.63	4.37	−114.71	−114.44	0.27

Note: $\Delta E_{solv1}=E_{solv(\mathbf{TS1})} - E_{solv(\mathbf{R1})}$; $\Delta E_{solv2}=E_{solv(\mathbf{TS2})} - E_{solv(\mathbf{R2})}$

Table 4 NPA charges of Cu cations of all complexes

	Cu(bpy)Br_2	Cu(L^1)Br_2	Cu(L^2)Br_2
SODM	1.05	1.02	1.01
R1	0.99	0.94	0.64
TS1	1.01	1.04	1.05
P1	0.62	0.66	0.59
SODMH	0.62	0.66	0.64
R2	1.03	1.06	1.05
TS2	1.07	1.08	1.06
P2	1.10	1.11	1.11

Conclusions

The systematic investigations at the DFT/UB3LYP level for $Cu(bpy)Br_2$ and its derivatives, $Cu(L^1)Br_2$ and $Cu(L^2)Br_2$ compounds, have theoretically confirmed the dismutation mechanisms of the SOD-like activities to be a redox cycle consisting of two half-reactions. In the first half-reaction, one proton is transferred from hydroperoxide radical (·OOH) to the N atom of one pyridine ring, while Cu(II) is reduced to Cu(I); In the second half-reaction, the same proton is transferred back to another hydroperoxide radical to form hydrogen peroxide molecule, oxidizing Cu(I) back to its initial state Cu(II). Based on the analysis of the forward Gibbs energy barriers, the SOD-like activities of these compounds increase gradually in the order of $Cu(bpy)Br_2 < Cu(L^1)Br_2 < Cu(L^2)Br_2$, which is consistent well with experimental results. The effective factors in affecting their SOD-like activities through the current theoretical investigations include the solvent effect, the structural and charged characteristics of different ligands, the flexibility of complex structures, and the electronic natures of their NBO orbitals. Such observations are useful for understanding and rationalizing the dismutation reaction activities of the SOD mimics with the center-copper-ion and some highly charged ligands.

Acknowledgment This work is supported by the National Science Foundation of China (No. 20673011, 20631020 and 20771017), the Major State Basic Research Development Programs (grant No. G2004CB719900).

References

1. Miller AF, Sorkin DL (1997) Superoxide dismutases: a molecular perspective. Comments Mol Cell Biophys 9:1–48
2. Orrell RW (2000) Neuromusscular Disord 10:63–68
3. Liochev SI, Fridovich I (2003) Mutant Cu, Zn superoxide dismutases and familial amyotrophic lateral sclerosis: evaluation of oxidative hypotheses. Free Radical Biol Med 34:1383–1389
4. Stathopulos PB, Rumfeldt JAO, Scholz GA, Irani RA, Frey HE, Hallewell RA, Lepock JR, Meiering EM (2003) Cu/Zn superoxide dismutase mutants associated with amyotrophic lateral sclerosis show enhanced formation of aggregates in vitro. Proc Nat Acad Sci USA 100:7021–7026
5. Valentine JS, Hart PJ (2003) Misfolded CuZnSOD and amyotrophic lateral sclerosis. Proc Nat Acad Sci USA 100:3617–3622
6. Bruns CK CK, Kopito RR (2007) Impaired post-translational folding of familial ALS-linked Cu, Zn superoxide dismutase mutants. EMBO J 26:855–866
7. Pelmenschikov V, Siegbahn PEM (2005) Copper-zinc superoxide dismutase: theoretical insights into the catalytic mechanism. Inorg Chem 44:3311–3320
8. Miller AF (2008) Redox tuning over almost 1 V in a structurally conserved active site: lessons from Fe-containing superoxide dismutase. Acc Chem Res 41:501–510
9. Pelmenschikov V, Siegbahn PEM (2006) Nickel superoxide dismutase reaction mechanism studied by hybrid density functional methods. J Am Chem Soc 128:7466–7475
10. Ohtsu H, Shimazaki Y, Odani A, Yamauchi O, Mori W, Itoh S, Fukuzumi S (2000) Synthesis and characterization of imidazolate-bridged dinuclear complexes as active site models of Cu, Zn-SOD. J Am Chem Soc 122:5733–5741
11. Jitsukawa K, Harata M, Arii H, Sakurai H, Masuda H (2001) SOD activities of the copper complexes with tripodal polypyridylamine ligands having a hydrogen bonding sites. Inorg Chim Acta 324:108–116
12. Heng F, Ying-Hua Z, Wei-Lin C, Zhuo-Ga D, Ming-Liang T, Liang-Nian J, Zong-Wan M (2006) Complexation, structure, and superoxide dismutase activity of the imidazolate-bridged dinuclear copper moiety with beta-cyclodextrin and its guanidinium-containing derivative. J Am Chem Soc 128:4924–4925
13. Hart PJ, Balbirnie MM, Ogihara NL, Nersissian AM, Weiss MS, Valentine JS, Eisenberg D (1999) A structure-based mechanism for copper-zinc superoxide dismutase. Biochem 38:2167–2178
14. Liu H, Zhu H, Eggers DK, Nersissian AM, Faull KF, Goto JJ, Ai J, Sanders-Loehr J, Gralla EB, Valentine JS (2000) Copper(2+) binding to the surface residue cysteine 111 of His46Arg human copper-zinc superoxide dismutase, a familial amyotrophic lateral sclerosis mutant. Biochem 39:8125–8132
15. Elam JS, Malek K, Rodriguez JA, Doucette PA, Taylor AB, Hayward LJ, Cabelli DE, Valentine JS, Hart PJ (2003) An alternative mechanism of bicarbonate-mediated peroxidation by copper-zinc superoxide dismutase: rates enhanced via proposed enzyme-associated peroxycarbonate intermediate. J Biol Chem 278:21032–21039
16. Danzeisen R, Achsel T, Bederke U, Cozzolino M, Crosio C, Ferri A, Frenzel M, Gralla EB, Huber L, Ludolph A, Nencini M, Rotilio G, Valentine JS, Carri MT (2006) Superoxide dismutase 1 modulates expression of transferrin receptor. J Biol Inorg Chem 11:489–498
17. Potter SZ, Zhu H, Shaw BF, Rodriguez JA, Doucette PA, Sohn SH, Durazo A, Faull KF, Gralla EB, Nersissian AM, Valentine JS (2007) Binding of a single zinc ion to one subunit of copper-zinc superoxide dismutase apoprotein substantially influences the structure and stability of the entire homodimeric protein. J Am Chem Soc 129:4575–4583
18. Ellerby LM, Cabelli DE, Graden JA, Valentine JS (1996) Copper-zinc superoxide dismutase: why not pH-dependent? J Am Chem Soc 118:6556–6561
19. Sreedhara A, Freed JD, Cowan JA (2000) Efficient inorganic deoxyribonucleases. Greater than 50-million-fold rate enhancement in enzyme-like DNA cleavage. J Am Chem Soc 122:8814–8824
20. Koevari E, Kraemer R (1996) Rapid phosphodiester hydrolysis by an ammonium-functionalized copper(II) complex. A model for the cooperativity of metal ions and nh-acidic groups in phosphoryl transfer enzymes. J Am Chem Soc 118:12704–12709
21. Hettich R, Schneider HJ (1997) Cobalt(III) polyamine complexes as catalysts for the hydrolysis of phosphate esters and of DNA. A measurable 10 million-fold rate increase. J Am Chem Soc 119:5638–5647
22. Salvemini D, Wang ZQ, Zweier JL, Samouilov A, MacArthur H, Misko TP, Currie MG, Cuzzocrea S, Sikorski JA, Riley DP (1999) A nonpeptidyl mimic of superoxide dismutase with therapeutic activity in rats. Sci 286:304–306
23. Fu H, Zhou YH, Chen WL, Deqing ZG, Tong ML, Ji LN, Mao ZW (2006) Complexation, structure, and superoxide dismutase activity of the imidazolate-bridged dinuclear copper moiety with beta-cyclodextrin and its guanidinium-containing derivative. J Am Chem Soc 128:4924–4925
24. Zhou YH, Fu H, Zhao WX, Chen WL, Su CY, Sun H, Ji LN, Mao ZW (2007) Synthesis, structure, and activity of supramolecular mimics for the active site and Arg141 residue of copper, zinc-superoxide dismutase. Inorg Chem 46:734–739
25. An Y, Tong ML, Ji LN, Mao ZW (2006) Double-strand DNA cleavage by copper complexes of 2, 2′-dipyridyl with electropositive pendants. Dalton Trans 17:2066–2071

26. Li JH, Wang JT, Hu P, Zhang LY, Chen ZN, Mao ZW, Ji LN (2008) Synthesis, structure and nuclease activity of copper complexes of disubstituted 2, 2′-bipyridine ligands bearing ammonium groups. Polyhedron 27:1898–1904
27. An Y, Hu P, Mao ZW. A new approach for constructing highly effective mimic of superoxide dismutase. Submitted
28. Garland MT, Grandjean D, Spodine E, Atria AM, Manzur J (1988) Structures of catena-di-m-chloro- and catena-di-m-bromo-(2, 2′-bipyridine) copper(II). Acta Crystallogr, Sect C: Cryst Struct Commun C44:1209–1212
29. Willett RD, Pon G, Nagy C (2001) Crystal chemistry of the 4, 4′-dimethyl-2, 2′-bipyridine/Copper Bromide System. Inorg Chem 40:4342–4352
30. Lee C, Yang W, Parr RG (1988) Development of the colle-salvetti correlation-energy formula into a functional of the electron density. Phys Rev B 37:785–789
31. Becke AD (1993) Density-functional thermochemistry. III. The role of exact exchange. J Chem Phys 98:5648–5652
32. Stevens PJ, Devlin FJ, Chablowski CF, Frisch MJ (1994) Ab initio calculation of vibrational absorption and circular dichroism spectra using density functional force fields. J Phys Chem 98:11623–11627
33. Hay PJ, Wadt WR (1985) Ab initio effective core potentials for molecular calculations. Potentials for the transition metal atoms scandium to mercury. J Chem Phys 82:270–283
34. Wadt WR, Hay PJ (1985) Ab initio effective core potentials for molecular calculations. Potentials for main group elements sodium to bismuth. J Chem Phys 82:284–298
35. Hay PJ, Wadt WR (1985) Ab initio effective core potentials for molecular calculations. Potentials for potassium to gold including the outermost core orbitals. J Chem Phys 82:299–310
36. Cances E, Mennucci B, Tomasi J (1997) A new integral equation formalism for the polarizable continuum model: theoretical background and applications to isotropic and anisotropic dielectrics. J Chem Phys 107:3032–3041
37. Mennucci B, Tomasi J (1997) Continuum solvation models: a new approach to the problem of solute's charge distribution and cavity boundaries. J Chem Phys 106:5151–5158
38. Mennucci B, Cances E, Tomasi J (1997) evaluation of solvent effects in isotropic and anisotropic dielectrics and in ionic solutions with a unified integral equation method: theoretical bases, computational implementation, and numerical applications. J Phys Chem B 101:10506–10517
39. Tomasi J, Mennucci B, Cances E (1999) THEOCHEM 464:211–226
40. Frisch MJ, Trucks GW, Schlegel HB, Scuseria GE, Robb MA, Cheeseman JR, Montgomery JA Jr, Vreven T, Kudin KN, Burant JC, Millam JM, Iyengar SS, Tomasi J, Barone V, Mennucci B, Cossi M, Scalmani G, Rega N, Petersson GA, Nakatsuji H, Hada M, Ehara M, Toyota K, Fukuda R, Hasegawa J, Ishida M, Nakajima T, Honda Y, OKitao NH, Klene M, Li X, Knox JE, Hratchian HP, Cross JB, Adamo C, Jaramillo J, Gomperts R, Stratmann RE, Yazyev O, Austin AJ, Cammi R, Pomelli C, Ochterski JW, Ayala PY, Morokuma K, Voth GA, Salvador P, Dannenberg JJ, Zakrzewski VG, Dapprich S, Daniels AD, Strain MC, Farkas O, Malick DK, Rabuck AD, Raghavachari K, Foresman JB, Ortiz JV, Cui Q, Baboul AG, Clifford S, Cioslowski J, Stefanov BB, Liu G, Liashenko A, Piskorz P, Komaromi I, Martin RL, Fox DJ, Keith T, Al-Laham MA, Peng CY, Nanayakkara A, Challacombe M, Gill PMW, Johnson B, Chen W, Wong MW, Gonzalez C, Pople JA (2003) Gaussian03. Gaussian, Inc, Pittsburgh, PA
41. Reedand AE, Weinhold F (1983) Natural bond orbital analysis of near-Hartree-Fock water dimer. J Chem Phys 78:4066–4073
42. Reed AE, Weinstock RB, Weinhold F (1985) Natural population analysis. J Chem Phys 83:735–746
43. Reedand AE, Weinhold F (1985) Natural localized molecular orbitals. J Chem Phys 83:1736–1740
44. Reed AE, Curtiss LA, Weinhold F (1988) Intermolecular interactions from anatural bond orbital, donor-acceptor view point. Chem Rev 88:899–926